AGU PUBLICATIONS

Geophysical Research Letters

RESEARCH LETTER
10.1002/2015GL064172

Key Points:
- NH-to-SH mean transit time increases from 1.1 years at Samoa to 1.4 years at the pole
- The width of the TTD varies little with SH latitude and is about 1.3 years
- Path-dependent and global lifetimes differ based on reactivity and transit time

Supporting Information:
- Texts S1–S3

Correspondence to:
M. Holzer,
mholzer@unsw.edu.au

Citation:
Holzer, M., and D. W. Waugh (2015), Interhemispheric transit time distributions and path-dependent lifetimes constrained by measurements of SF_6, CFCs, and CFC replacements, *Geophys. Res. Lett.*, *42*, doi:10.1002/2015GL064172.

Received 8 APR 2015
Accepted 6 MAY 2015
Accepted article online 11 MAY 2015

Interhemispheric transit time distributions and path-dependent lifetimes constrained by measurements of SF_6, CFCs, and CFC replacements

Mark Holzer[1,2] and Darryn W. Waugh[3]

[1]Department of Applied Mathematics, School of Mathematics and Statistics, University of New South Wales, Sydney, New South Wales, Australia, [2]Also at Department of Applied Physics and Applied Mathematics, Columbia University, New York, New York, USA, [3]Department of Earth and Planetary Sciences, Johns Hopkins University, Baltimore, Maryland, USA

Abstract We constrain tropospheric transport from Northern Hemisphere midlatitudes to the Southern Hemisphere (SH) surface using measurements of SF_6, CFCs, and CFC replacement gases and a novel maximum-entropy-based inversion approach. We provide the first estimate of the width Δ of the tropospheric interhemispheric transit time distribution (TTD). We find that Δ has a value of $\sim$1.3 years that varies little with SH latitude, compared to the mean transit time Γ that increases from $\sim$1.1 years in the SH tropics to $\sim$1.4 years at the South Pole. The TTD shape parameter Δ/Γ is thus larger in the SH tropics than at middle and high SH latitudes. Our analysis introduces a simple path-dependent lifetime that parameterizes chemical losses. The path-dependent lifetimes are estimated for CFC replacements, and systematic differences between path-dependent and global lifetimes are interpreted. The path-dependent lifetimes have the potential to provide new observational constraints on tropospheric and stratospheric loss processes.

1. Introduction

The measured trace gas concentrations from global networks of surface stations provide a great deal of information not only on the abundance of these gases but also on their sources, the integrated loss processes acting on these gases, and on the fundamental transport fluxes within the atmosphere. While many studies have exploited these measurements to infer radiative forcings [e.g., *Naik et al.*, 2000; *Montzka et al.*, 2009], to constrain sources [e.g., *Stohl et al.*, 2009; *Fortems-Cheiney et al.*, 2013], and to estimate global-mean lifetimes [e.g., *Engel et al.*, 2013, and references therein], the constraints that these measurements provide for transport have been relatively little explored.

Here we use measurements of a suite of tracers (SF_6, CFCs, and CFC replacement gases) to (i) constrain the tropospheric transport from the Northern Hemisphere (NH) midlatitudes to the Southern Hemisphere (SH) and, relatedly, to (ii) infer the loss of CFC replacement gases en route to the SH, parameterized as an effective lifetime.

Recently, *Waugh et al.* [2013] showed that SF_6 tracer ages strongly constrain the mean transit time from NH source regions because of the nearly linear time dependence of SF_6 concentrations. However, *Waugh et al.* [2013] did not directly infer mean transit time, but only computed the SF_6 tracer age, which changes in time even for steady flow due to changes in growth rate. Here we analyze multiple species to constrain both the mean and variance of the transit time distribution (TTD), a tracer-independent fundamental characteristic of atmospheric transport. To the best of our knowledge, we provide the first observation-based estimate of the variance of the TTD (expressed as a TTD width, defined below) in the troposphere.

A key property of tracers is their chemical lifetime, which together with dilution through physical transport determines the concentration of transient gases. For CFC replacements (hydrochlorofluorocarbons (HCFCs) and hydrofluorocarbons (HFCs)) the lifetimes are set primarily by reaction with hydroxyl radical (OH) in the lower tropical troposphere where OH concentrations and temperature are high enough to activate large reaction rates [e.g., *Lawrence et al.*, 2001]. Chemical lifetime is typically specified in terms of a global bulk timescale (for a review, see *Plumb et al.* [2013]). While global lifetime is defined by a global weighted average of the local

loss frequencies, the integrated loss that a tracer experiences during its transit through the troposphere to the point of measurement ("field point") depends on the transport paths through the poorly known loss field. Here we parameterize this path-dependent integrated loss by a timescale that depends on source and field point and use measurements from the "Halocarbons and other Atmospheric Trace Species Group" (HATS) station network to estimate this path-dependent lifetime for HCFCs and HFCs for transport from the NH midlatitudes to the SH surface.

We find that the TTD is broader at Samoa than at either Tasmania or the South Pole, which have similar TTD shape parameters. This unexpected result highlights the subtle interplay between fast transport pathways and slow eddy-diffusive recirculations controlling the mode and tails of the TTD, respectively. Our results suggest that for gases with lifetimes of order 10 years, the path-dependent lifetimes in the SH can be up to 30% longer than the global lifetimes, with longer path-dependent lifetimes corresponding to longer mean transit times, while for HFC152a with a lifetime of order 1 year, the path-dependent lifetime is ~40% shorter.

2. Method and Data

We consider multiple trace gases with concentrations χ_j, where $j = 1 \ldots J$ identifies the species. Given the surface concentrations $\chi_j^S(\mathbf{r}_s, t_s)$ over the source region as a function of surface location $\mathbf{r}_s$ and source time t_s and parameterizing the path-dependent loss with timescale τ_j^c, the concentrations outside the source region at field points $\mathbf{r}$ can be obtained by convolving χ_j^S with the boundary propagator $\mathcal{G}$ [e.g., *Holzer and Hall*, 2000]:

$$\chi(\mathbf{r}, t) = \int_0^\infty \mathrm{d}\xi \int d^2 r_s \, \mathcal{G}(\mathbf{r}, t|\mathbf{r}_s, t-\xi) \chi_j^S(\mathbf{r}_s, t-\xi) e^{-\xi/\tau_j^c(\mathbf{r},t)} \quad , \tag{1}$$

where τ_j^c varies with field point and time $(\mathbf{r}, t)$ but is defined to be independent of transit time, ξ.

With only a few NH stations, the spatial dependence of χ_j^S is poorly observed. We assume that in the SH the $\mathbf{r}_s$ dependence of χ_j^S within the NH midlatitudes can be neglected and simply replace χ_j^S with an average NH midlatitude concentration χ_j^{NH}. Equation (1) then reduces to a convolution in time only:

$$\chi_j(\mathbf{r}, t; G) = \int_0^\infty \mathrm{d}\xi \, G(\mathbf{r}, t|t-\xi) \chi_j^{\mathrm{NH}}(t-\xi) e^{-\xi/\tau_j^c(\mathbf{r},t)} \quad , \tag{2}$$

where $G = \int d^2 r_s \, \mathcal{G}$ is the transit time distribution (TTD) with normalization $\int_0^\infty G \, \mathrm{d}\xi = 1$. We do not assume stationary flow and hence retain explicit dependence of G on both t and ξ. The loss frequency experienced by a tracer molecule varies along its path from the source to $(\mathbf{r}, t)$. We regard the lifetime $\tau_j^c(\mathbf{r}, t)$ in (2) as an effective inverse loss frequency that parameterizes the integrated loss over all possible paths to $(\mathbf{r}, t)$. Because the transport paths depend on field point $(\mathbf{r}, t)$ for a given source distribution, τ_j^c will generally depend on $(\mathbf{r}, t)$.

We now consider two types of inverse problems that we apply alternately to different sets of gases as detailed in section 3. (i) Given the NH time series $\chi_j^{\mathrm{NH}}(t-\xi)$ and field point measurements $\chi_j^{\mathrm{obs}}(\mathbf{r}, t)$ at a given point $\mathbf{r}$ (i.e., surface station in the SH) for J species with known lifetimes τ_j^c, we estimate the TTD by deconvolving the constraints that the G-propagated concentrations (2) must match the observations:

$$\chi_j^{\mathrm{obs}}(\mathbf{r}, t) = \chi_j(\mathbf{r}, t; G) \quad . \tag{3}$$

(ii) Given an estimate of G from a subset of the species considered, we solve the constraints (3) for the remaining tracers for their path-dependent lifetimes τ_j^c. Inverse problem (ii) requires solving for each species one equation (3) for the single unknown τ_j^c, which is straightforward using standard numerical algorithms.

Inverse problem (i) is more involved because the functional form of G must be estimated from only a finite number of constraints. This classic underdetermined deconvolution problem can be regularized by assuming that G can be parameterized with a number of parameters less than or equal to the number of tracer constraints, J. One could assume that G is an inverse Gaussian (IG) and hence a function of only two parameters (mean and variance). However, using an IG, it is in practice difficult to find solutions that are physical and consistent across the available field times t.

Here we adopt a functional form for G that results from maximizing the information entropy of G subject to error-free tracer constraints [e.g., *Holzer et al.*, 2010]:

$$G(t, t-\xi; \mu, \{\lambda_j\}) = \frac{\mu(\xi)}{Z} \exp\left(- \sum_j \lambda_j(t) \chi_j^{\mathrm{NH}}(t-\xi)\, e^{-\xi/\tau_j^c} \right) \quad , \tag{4}$$

where the λ_j are J parameters to be determined from the J constraints (3), μ is a prior guess at G (prior, for short) to which G reduces in the absence of data constraints ($\lambda_j = 0$), and Z is a normalization constant. To account for the uncertainty in the trace gas measurements, we generate several randomly perturbed synthetic copies of the measurements and solve the tracer constraints for the λ_j in a least squares sense (see supporting information (SI) for details). We also add random Gaussian error of 10% amplitude to the lifetimes. To estimate the uncertainty due to the inherently underdetermined nature of the deconvolution [e.g., *Holzer et al.*, 2010], we perform the inversion for an ensemble of randomly chosen priors; see the SI for details.

2.1. Data

We use monthly averages for SF_6, CFC-11, CFC-12, CFC-113, HCFC-22, HCFC-141b, HCFC-142b, HFC-134a, and HFC-152a obtained from the HATS station network. The time series $\chi_j^{\mathrm{NH}}(t)$ for the NH *midlatitudes* are estimated as three-station (Trinidad Head, CA; Niwot Ridge, CO; and Mace Head, Ireland) averages. We perform inversions for stations SPO (South Pole), CGO (Tasmania, 40°S, 145°E), and SMO (Samoa, 14°S, 171°W). We focus on 2006–2011 to infer the path-dependent lifetimes and on 2000–2005 to constrain the TTD (see SI for details).

3. Strategy and Illustration for Synthetic Tracers

To test our method, we apply it to synthetic data obtained by propagating χ_j^{NH} with a known IG TTD that is completely determined by its mean, Γ, and width, Δ, defined for any TTD G through $\Gamma \equiv \int_0^\infty \mathrm{d}\xi\, \xi\, G(\xi)$ and $\Delta^2 \equiv \frac{1}{2}\int_0^\infty \mathrm{d}\xi\, (\xi-\Gamma)^2\, G(\xi)$. Without noise and assuming zero error in the lifetimes, the inversion recovers Γ and Δ to within a few percent given two or more tracer constraints.

The synthetic case is less straightforward when we add noise to the concentrations and lifetimes to account for their uncertainties. Because there is little variation in the growth rates of SF_6 and CFCs since 2000, the transport information contained in these tracers is strongly degraded by the uncertainty in their concentrations, accounted for here by the noise. While SF_6 strongly constrains Γ, we find that the addition of CFCs does not allow for an unbiased estimate of Δ. It is therefore necessary to use one or more of the CFC replacement gases to constrain transport accurately. Before this can be done, we need to know the lifetimes τ_j^c in the convolution integral (2), which are generally not equal to the global lifetimes. Fortunately, as demonstrated below, the inversion for the lifetimes is insensitive to knowing the precise TTD. Therefore, our strategy is as follows:

1. We use SF_6 and the three CFCs for a first estimate of the TTD (inversion type (i)). For this step we use the known global lifetimes [*Ko et al.*, 2013] for the τ_j^c of the CFCs and SF_6 because these are very long (several decades to millennia) on the scale of tropospheric transport.
2. We use this first estimate of the TTD to determine the τ_j^c of the CFC replacements (inversion type (ii)).
3. We use the CFC replacements, now that we know their τ_j^c, together with SF_6 for a refined estimate of the TTD (inversion type (i)). While we estimate τ_j^c at every field time t, the ensemble spread is typically larger than seasonal and interannual variations. We therefore time average τ_j^c for step (c) and drop its t dependence below.

Figure 1a demonstrates to what degree the lifetimes of the HCFC and HFC gases can be recovered for synthetic tracers using SF_6 and the three CFCs to constrain the transport. We consider three synthetic TTDs: IGs with $\Gamma = 1.3$ years, and $\Delta/\Gamma = 3/4$, 1, and 4/3. For $\Delta/\Gamma = 1$, we recover the lifetimes of the CFC replacements to within 1%, except for HFC-152a for which the error is 5%. For $\Delta/\Gamma = 3/4$, the lifetimes are underestimated by 5 to 15%, and for $\Delta/\Gamma = 4/3$, they are overestimated by 7 to 37%, with the largest errors for HFC-152a. However, in all cases our error bars overlap the correct value. The error magnitude is not simply a function of lifetime but also depends on the shape of the χ_j^{NH} time series and the noise amplitude. Biases are largest for HFC152a because the short-ξ dependence of G is particularly poorly constrained by SF_6 and the CFCs. Fortunately, the real atmosphere's TTD at SH stations is estimated below to have a Δ/Γ in the range 0.88–1.12 so that estimated lifetimes should be accurate to within ~10%.

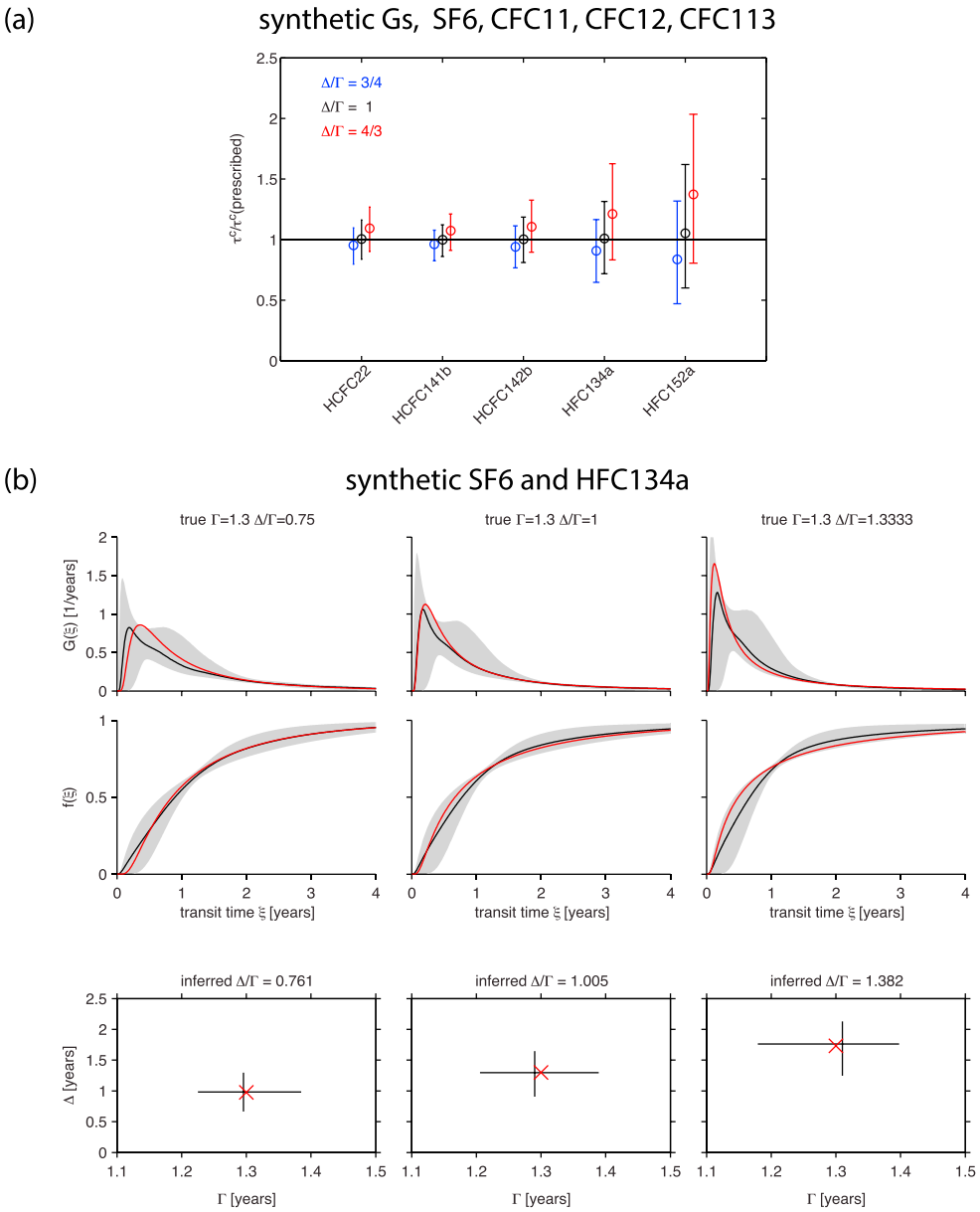

Figure 1. (a) Ratio of inferred to prescribed lifetimes for synthetic IG TTDs with $\Gamma = 1.3$a and $\Delta/\Gamma = 3/4$, 1, and 4/3 and corresponding synthetic SF_6, CFC-11, CFC-12, and CFC-113 tracer constraints. (b) Estimates of the TTD $G(\xi)$ (top panels), of $f(\xi) \equiv \int_0^\xi G(\xi')\,d\xi'$ (middle panels), and of Γ and Δ (bottom panels), using synthetic SF_6 and HFC-134a. Prescribed ("true") quantities are plotted in red; inferred quantities, in black (ensemble spread shaded grey).

To constrain the TTD width Δ, it turns out that HFC-134a has the greatest sensitivity to Δ for the field times considered. This can be seen, for example, by plotting the convolved synthetic tracer concentration as a function of Γ and Δ of the assumed IG propagator (not shown). We therefore use SF_6 plus HFC-134a to constrain Δ. Using the other tracers as additional constraints tends to bias our estimates because the uncertainties (noise in the synthetic case) tend to make a wide range of Δ/Γ compatible with the tracer constraints.

Figure 1b shows the ensemble-averaged estimates of the TTD, of the cumulative TTD $f(\xi) \equiv \int_0^\xi d\xi'\, G(\xi')$, and of Γ and Δ. Physically, $f(\xi)$ at $\mathbf{r}$ is the local fraction of fluid elements whose transit times to $\mathbf{r}$ are less than ξ. Figure 1b shows results for the same three synthetic cases considered in Figure 1a. Unsurprisingly, with only two usable tracer constraints, the inferred TTD does not exactly match the true TTD in any of the cases, and the ensemble spread (grey shading) at any given ξ is large. The closest match with these particular tracer constraints happens to occur for $\Delta/\Gamma = 1$. The largest discrepancies occur near the mode of the TTD, with

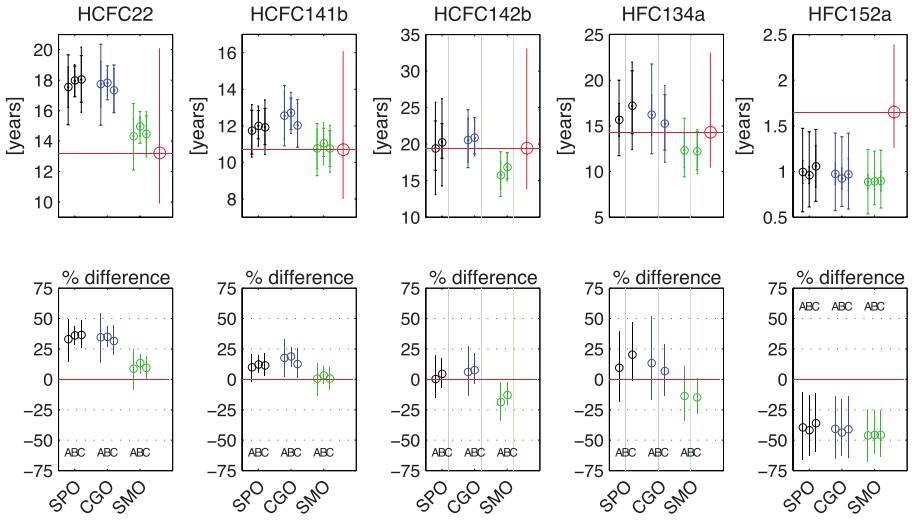

Figure 2. Inferred path-dependent lifetimes τ^c at SPO (black), CGO (blue), and SMO (green) for sets A, B, and C of tracer constraints, as described in the text. Error bars with larger end caps represents the ensemble spread; those with small end caps are the standard deviation of the monthly values from the multiyear mean. The global lifetimes $\overline{\tau}$ relative to OH [*Engel et al.*, 2013] are plotted in red. The bottom row shows the percentage difference between τ^c and $\overline{\tau}$.

the early-time TTD being overestimated for $\Delta/\Gamma < 1$ and underestimated for $\Delta/\Gamma > 1$. However, Γ and Δ are recovered nearly perfectly in all cases. The most likely values are within 2% of the true value, and the ensemble spread (half the error bar length) is ~7% and ~30% for Γ and Δ, respectively. The synthetic tracers thus provide some confidence that we can obtain unbiased estimates of Γ and Δ.

4. Inversion Results for HATS Data

4.1. Path-Dependent Lifetimes

Figure 2 shows three estimates of the path-dependent lifetimes τ_j^c of the CFC replacements, each estimate corresponding to a different set of tracer constraints. Because the τ_j^c of CFC replacements estimated from SF_6, CFC-11, CFC-12, and CFC-113 ("estimate A") are used to constrain transport using CFC replacements below, it is essential that these lifetimes are validated for consistency. We therefore also used SF_6 and HFC-134a ("estimate B") with its lifetime from estimate A to infer the τ_j^c of the other CFC replacements and similarly SF_6 and HCFC-142b ("estimate C") with its lifetime from estimate A to validate the other lifetimes, including that of HFC-134a. We chose HCFC-142b and HFC-134a because they have the greatest sensitivity to Δ for IG synthetic transport. Figure 2 shows consistency among the estimates, with differences that are an order of magnitude smaller than the ensemble spread. It is therefore legitimate to use the estimate A lifetimes for constraining the TTD and to interpret the lifetimes themselves.

Figure 2 shows the systematic variations of τ_j^c for the CFC replacements with respect to species and station and underscores the path-dependent nature of τ_j^c. Except for HFC-152a, the τ_j^c lie within the broad uncertainty ranges of the Stratospheric Processes and their Role in Climate global lifetimes $\overline{\tau_j}$ [*Engel et al.*, 2013], although for all species there are systematic variations. The systematics of $\tau_j^c < \overline{\tau_j}$ for $\overline{\tau_j}$ ~1 year, and of longer τ_j^c corresponding to longer Γ for $\overline{\tau_j}$ ~10 years, are set by the interplay of transport and loss timescales and are fundamental to the system.

To get insight into the systematics of Figure 2 and into how the path-dependent and global lifetimes differ by virtue of their definitions, we consider key limits for a simple conceptual model. This model has steady state tracer concentrations, only NH sources that maintain a constant mixing ratio χ^{NH} in the lower extratropical NH, a long local background lifetime τ_B outside the low-level tropics, and a local lifetime τ_T inside the low-level tropics. For simplicity, we further postulate rapid vertical exchange so that all paths to the SH sample the lower tropics. Suppressing species index j, the path-dependent lifetime τ^c is defined by (2), while the global lifetime $\overline{\tau}$ is defined in terms of the global average of the local loss frequencies $[\tau(\mathbf{r})]^{-1}$ [*Plumb et al.*, 2013]:

$$\frac{1}{\overline{\tau}} \equiv \frac{\int [\tau(\mathbf{r})]^{-1} \chi(\mathbf{r}) \rho(\mathbf{r}) d^3r}{\int \chi(\mathbf{r})\, \rho(\mathbf{r})\, d^3r} \quad , \tag{5}$$

where $\tau(\mathbf{r})$ is the local lifetime at $\mathbf{r}$ and ρ is air density.

First, consider the fast limit $\tau_T \to 0$. The concentrations in the lower tropics then go to zero, and because in our conceptual model all paths to the SH must pass through the lower tropics, the SH extratropical concentrations, χ^{SH}, also go to zero. Because $\chi^{NH} \int_0^\infty G(\xi) \exp(-\xi/\tau^c) d\xi$ must match χ^{SH}, the path-dependent lifetime τ^c must go to zero in both the SH and in the tropics. However, because the tropical concentration χ_T becomes proportional to τ_T for small τ_T while χ^{NH} remains fixed, it follows from (5) that $\overline{\tau}$ approaches a finite limit as $\tau_T \to 0$. Thus, in the limit of tropical loss that is fast compared to the meridional transport timescale, $\tau^c < \overline{\tau}$.

A simple conceptual limit for which $\tau^c(\mathbf{r}) = \overline{\tau}$ is the case of spatially uniform loss $\tau_T \to \tau_B$. Although this does not apply to the gases considered here for which τ_T/τ_B is set primarily by the ratio of extratropical to tropical OH concentrations, this second limit shows that it is possible for path-dependent and global lifetimes to coincide. In general, however, $\tau^c(\mathbf{r})$ is expected to differ from $\overline{\tau}$. For $\tau_{ex} < \tau_T < \tau_B$, where τ_{ex} is the horizontal exchange time between the tropics and extratropics, the ratio $\tau^c(\mathbf{r})/\overline{\tau}$ can be either greater or less than unity depending on the value of τ_T/τ_B and the location of $\mathbf{r}$ relative to the structure of the transport and the distribution of loss frequencies.

In general, the smaller the integrated loss en route to $\mathbf{r}$, the longer $\tau^c(\mathbf{r})$. Because it follows from (2) that the integrated loss depends to first order on $\exp[-\Gamma(\mathbf{r})/\tau^c(\mathbf{r})]$ for $\tau^c \gg \Gamma$, a given integrated loss must have longer $\tau^c(\mathbf{r})$ for longer $\Gamma(\mathbf{r})$. In other words, if concentrations were to remain intact after passing through the high-loss tropics, their preservation over increasing transit times would be reflected in correspondingly increasing path-dependent lifetimes.

The systematics of $\tau^c < \overline{\tau}$ for highly reactive species, and of longer $\tau^c(\mathbf{r})$ corresponding to longer $\Gamma(\mathbf{r})$ for longer-lived species, is born out in Figure 2. For HFC-152a with a global lifetime $\overline{\tau}$ of only ~1.6 years (and hence a much shorter local lifetime τ_T in the lower tropics), $\tau^c < \overline{\tau}$, consistent with our expectations from the short-τ_T limit. For the other CFC replacement gases of ~10 year lifetimes, the differences between τ^c and $\overline{\tau}$ are less dramatic, but for all species the values of τ^c at SPO and CGO are longer than at SMO as expected from the longer mean transit times to SPO and CGO, given that their loss occurs predominantly in the tropics.

The details of the path-dependent lifetimes depend on loss processes throughout the atmosphere, including the stratosphere: Up to 20% of air undergoing interhemispheric surface-to-surface transport is estimated to pass through the stratosphere [*Holzer*, 2009], where photolysis may be significant for some species.

4.2. Mean Transit Time, Γ, and TTD Width, Δ

Having estimated and cross validated the loss timescales τ_j^c of CFC replacements, we now return to constraining the TTD itself. We use HFC-134a (in addition to SF_6) because in the context of a synthetic IG TTD, it constrains Δ without bias. With only two tracers, the full TTD remains highly uncertain, with uncertainty bounds (not shown) similar to the synthetic cases of Figure 1b. We therefore focus on Γ and Δ, i.e., on the first two centered moments of the TTD. With these tracers, Γ is well constrained over the full 2000–2011 period considered, while Δ is much better constrained for 2000–2005.

Figure 3a shows the estimated time series of Γ, with 12 year means of 1.44, 1.41, and 1.10 years at SPO, CGO, and SMO, respectively. As expected, Γ to SMO is shorter (by ~3–4 months) than Γ to the SPO and CGO because SMO is closer to the NH source region. Γ exhibits greater seasonality and interannual variations at SMO than at CGO and SPO, which is partly due to interhemispheric tracer gradients being sharpest across the tropics. The apparent downward trend of Γ at SMO after ~2001 may be an artifact of trends in the distribution of the SF_6 sources [*Patra et al.*, 2011].

The seasonality of Γ at SMO is consistent with the seasonality of the Hadley cell. During boreal summer, trace gases of midlatitude origin are drawn into the Intertropical Convergence Zone (ITCZ) in the NH and enter the SH aloft, while during boreal winter the zonally averaged ITCZ is in the SH and the surface inflow into this convergence provides a fast path across the equator [e.g., *Prinn et al.*, 1992; *Holzer*, 1999; *Bowman and Erukhimova*, 2004; *Holzer*, 2009]. Consequently, in boreal summer the tropical SH would be expected to see longer mean transit times to allow for the mixing down and recirculation to the surface, with the most direct transport missing Samoa. By contrast, in boreal winter we would expect faster transport to the SH tropical surface with the inflow to the ITCZ. This is just the seasonality that Γ shows at SMO, with a difference of about 2–3 months between winter and summer.

At CGO and SPO, Γ shows some variability with a suggestion of a seasonal signal for 2000–2004. However, there is a lack of year-to-year coherence, and for field times later than 2004, the variations in the most probable values of Γ are comparable in magnitude to the size of the uncertainty bounds. This suggests that some of

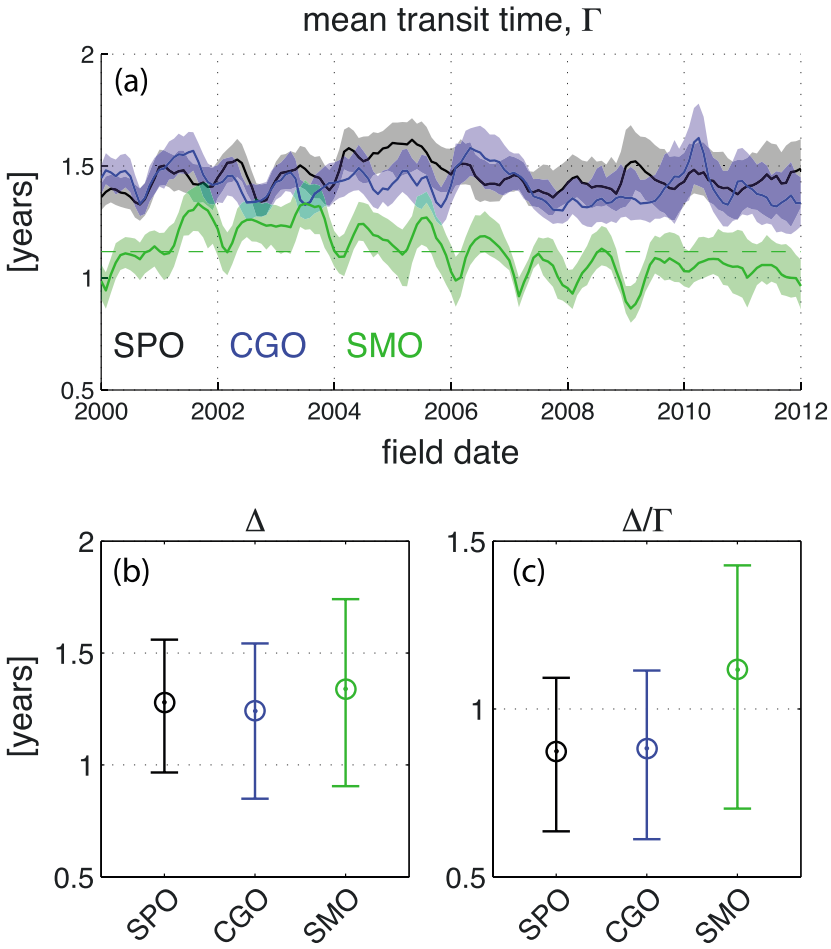

Figure 3. (a) The mean transit time Γ to stations SPO (South Pole), CGO (Tasmania), SMO (Samoa). The shaded error bands represent the spread over the ensemble of priors. (b) The corresponding TTD width Δ and (c) shape parameter Γ/Δ. Error bars combine ensemble spread and monthly variability for 2000–2005.

the variations in Γ at these stations could be artifacts representing variations in tracer concentrations instead of variations in transport. We will therefore not further examine the variability at CGO and SPO.

Figure 3b shows the inferred TTD width Δ, with error bars that represent the combined spread due to the prior ensemble and due to variations in the monthly estimates across the period 2000–2005. Within their uncertainties, the values of Δ at the three stations are roughly equal: $\Delta = 1.28$, 1.24, and 1.34 years for SPO, CGO, and SMO, respectively. However, the shape of the TTD is governed by the ratio Δ/Γ, with Γ merely setting the timescale for the transit time dependence of *G*. As shown in Figure 3c, the most probable value of Δ/Γ shows systematic variation with latitude, with SPO and GCO having nearly identical values of $\Delta/\Gamma = 0.88$, while SMO has $\Delta/\Gamma = 1.12$. Thus, relative to the mean, the TTD is 27% broader at SMO than in the middle- and high-latitude SH, where our results suggest small gradients in Δ/Γ. These systematics are similar to those seen in numerical integrations with chemical transport models (C. Orbe, personal communication, 2014). Our interpretation of the TTD being broader in the tropics is that the fast early signal from the NH sources results in a relatively low mean, while the tails of the TTD due to recirculations within the NH result in a broad tail that leads to a wider TTD relative to the mean than is the case in the SH middle and high latitudes, where the fast early NH signal is absent.

5. Conclusions

We applied inverse modeling to multiple tracers to constrain tropospheric transport from NH midlatitudes to the SH and provided the first estimate of the width of the corresponding TTD. Our analysis also intro-

duces a path-dependent lifetime $\tau^c(\mathbf{r})$ that parameterizes the integrated loss during transport to **r**. Our central conclusions are as follows:

1. The mean transit time from the NH midlatitude surface increases from $\Gamma \sim 1.1$ years at Samoa to $\Gamma \sim 1.4$ years at the South Pole as expected, but with only small differences between Tasmania and the South Pole, suggesting weak gradients in Γ from middle to high southern latitudes. At Samoa, Γ displays strong seasonality consistent with the annual cycle of the Hadley-Walker circulation, while seasonality is suppressed at higher latitudes.
2. The width Δ of the TTD varies much less with latitude than Γ so that the TTD shape parameter Δ/Γ varies primarily with $1/\Gamma$, being about 27% larger at Samoa than at Tasmania and the South Pole. Relative to the mean, the TTD is hence broader at Samoa than at high southern latitudes, likely due to slow recirculations imparting long tails to a TTD with an early peak due to fast transport from the NH that is absent at high southern latitudes.
3. The path-dependent lifetimes $\tau^c(\mathbf{r})$ generally differ from the corresponding global lifetimes, $\overline{\tau}$. The $\tau^c(\mathbf{r})$ depend subtly on how long the tracer spends in key loss regions on its way to point **r**. For HFC-152a with a tropical lifetime short compared to the large-scale transport times, $\tau^c(\mathbf{r})$ is ~40% shorter than $\overline{\tau}$ throughout the SH. For CFC replacements with global lifetimes on the order of a decade, we find that $\tau^c(\mathbf{r})$ varies systematically with mean transit time $\Gamma(\mathbf{r})$, with longer $\Gamma(\mathbf{r})$ corresponding to longer $\tau^c(\mathbf{r})$.

We acknowledge several sources of uncertainty that warrant further research. Representing the NH midlatitude concentrations by a three-station average ignores potentially important spatial gradients within the source region and likely does not represent the full time dependence of the source region concentrations. This limits our ability to extract transport information from the seasonal and interannual variations of the measured SH concentrations, as evidenced by our substantial ensemble spreads. Also, our parameterization of chemical loss as exponential decay with transit time relative to a time-averaged lifetime τ^c is an oversimplification for short lifetimes whose limitations need to be examined further in future theoretical studies.

Future work will extend our analysis to additional trace gas measurements from the "Advanced Global Atmospheric Gases Experiment" (AGAGE) surface network and from recent aircraft campaigns (e.g., High-performance Instrumented Airborne Platform for Environmental Research Pole-to-Pole Observations (HIPPO) [*Wofsy*, 2011]). This will further constrain tropospheric transport and provide valuable metrics, such as the path-dependent lifetimes and the mean and width of the TTD throughout the troposphere, against which to validate global atmosphere-chemistry models. A strength of the empirical approach to lifetimes adopted here is that it allows us to formulate a relatively straightforward inverse problem for the interhemispheric TTD using only available observations without any additional modeling. Future estimates of the path-dependent lifetimes for a number of tracers and locations within the troposphere will provide direct observation-based constraints on the OH distribution of the troposphere.

Acknowledgments
This work was supported by grants ARC DP120100674 (M.H.), NSF AGS-1402931 (M.H.), NSF AGS-1403676 (D.W.), and NASA NNX14AP58G (D.W.). We thank Steven Montzka for helpful discussions regarding the HATS data. All data used are available at http://www.esrl.noaa.gov/gmd/hats/data.html.

The Editor thanks two anonymous reviewers for their assistance in evaluating this paper.

References

Bowman, K. P., and T. Erukhimova (2004), Comparison of global-scale Lagrangian transport properties of the NCEP reanalysis and CCM3, *J. Clim.*, *17*, 1135–1146.

Engel, A., et al. (2013), SPARC 2013, chapter 4: Inferred lifetimes from observed trace-gas distributions, *Tech. Rep. 6, WCRP-15/2013*, World Clim. Res. Programme, Zurich, Switzerland.

Fortems-Cheiney, A., F. Chevallier, M. Saunois, I. Pison, P. Bousquet, C. Cressot, H. J. Wang, Y. Yokouchi, and F. Artuso (2013), HCFC-22 emissions at global and regional scales between 1995 and 2010: Trends and variability, *J. Geophys. Res. Atmos.*, *118*, 7379–7388, doi:10.1002/jgrd.50544.

Holzer, M. (1999), Analysis of passive tracer transport as modeled by an atmospheric general circulation model, *J. Clim.*, *12*, 1659–1684.

Holzer, M. (2009), The path density of interhemispheric surface-to-surface transport: Part II. Transport through the troposphere and stratosphere diagnosed from NCEP data, *J. Atmos. Sci.*, *66*, 2172–2189, doi:10.1175/2009JAS2895.1.

Holzer, M., and T. M. Hall (2000), Transit-time and tracer-age distributions in geophysical flows, *J. Atmos. Sci.*, *57*, 3539–3558.

Holzer, M., F. W. Primeau, W. M. Smethie Jr., and S. Khatiwala (2010), Where and how long ago was water in the western North Atlantic ventilated? Maximum-entropy inversions of bottle data from WOCE line A20, *J. Geophys. Res.*, *115*, C07005, doi:10.1029/2009JC005750.

Ko, M., P. Newman, S. Reimann, and S. Strahan (2013), SPARC 2013: Report on lifetimes of stratospheric ozone-depleting substances, their replacements, and related species, *Tech. Rep. 6, WCRP-15/2013*. World Clim. Res. Programme, Zurich, Switzerland.

Lawrence, M. G., P. Jöckel, and R. von Kuhlmann (2001), What does the global mean OH concentration tell us?*Atmos. Chem. Phys.*, *1*, 37–49.

Montzka, S. A., B. D. Hall, and J. W. Elkins (2009), Accelerated increases observed for hydrochlorofluorocarbons since 2004 in the global atmosphere, *J. Geophys. Res.*, *36*, L03804, doi:10.1029/2008GL036475.

Naik, V., A. K. Jain, K. O. Patten, and D. J. Wuebbles (2000), Consistent sets of atmospheric lifetimes and radiative forcings on climate for CFC replacements: HCFCs and HFCs, *J. Geophys. Res.*, *105*(D5), 6903–6914.

Patra, P. K., et al. (2011), Transcom model simulations of CH4 and related species: Linking transport, surface flux and chemical loss with CH4 variability in the troposphere and lower stratosphere, *Atmos. Chem. Phys.*, *11*, 12,813–12,837, doi:10.5194/acp-11-12813-2011.

Plumb, R. A., R. S. Stolarski, M. I. Hegglin, M. J. Prather, and C. M. Volk (2013), SPARC 2013, chapter 2: The theory of estimating lifetimes using models and observations, *Tech. Rep. 6, WCRP-15/2013*, World Clim. Res. Programme, Zurich, Switzerland.

Prinn, R., et al. (1992), Global average concentration and trend for hydroxyl radicals deduced from ALE/GAGE trichloroethane (methyl chloroform) data for 1978–1990, *J. Geophys. Res.*, *97*, 2445–2461.

Stohl, A., et al. (2009), An analytical inversion method for determining regional and global emissions of greenhouse gases: Sensitivity studies and application to halocarbons, *Atmos. Chem. Phys.*, *9*, 1597–1620.

Waugh, D. W., et al. (2013), Tropospheric SF6: Age of air from the Northern Hemisphere midlatitude surface, *J. Geophys. Res. Atmos.*, *118*, 11,429–11,441, doi:10.1002/jgrd.50848.

Wofsy, S. C. (2011), HIAPER Pole-to-Pole Observations (HIPPO): Fine-grained, global-scale measurements of climatically important atmospheric gases and aerosols, *Philos. Trans. R. Soc. A*, *369*, 2073–2086, doi:10.1098/rsta.2010.0313.